Opposite polarity programs regulate asymmetric subsidiary cell divisions in grasses

Dan Zhang[1], Emily B. Abrash[2], Tiago D. G. Nunes[1], Ines Hidalgo Prados[1], M. Ximena Anleu Gil[2], Barbara Jesenofsky[1], Heike Lindner[1], Dominique C. Bergmann[2,3,*], Michael T. Raissig[1,4,5,*]

[1] Centre for Organismal Studies Heidelberg, Heidelberg University, Heidelberg, Germany
[2] Department of Biology, Stanford University, Stanford, CA 94305, USA
[3] Howard Hughes Medical Institute, Stanford University, Stanford, CA 94305, USA
[4] Institute of Plant Sciences, University of Bern, Bern, Switzerland

[5] lead contact
* correspondence: dbergmann@stanford.edu (D.C.B.), michael.raissig@ips.unibe.ch (M.T.R.)

Stomata are cellular pores on the leaf epidermis that Grass stomata recruit lateral subsidiary cells (SCs), which are key to the unique stomatal morphology and the efficient plant-atmosphere gas exchange in grasses. Subsidiary mother cells (SMCs) strongly polarise before an asymmetric division forms a SC. Yet apart from a proximal polarity module that includes PANGLOSS1 (PAN1) and guides nuclear migration, little is known regarding the developmental processes that form SCs. Using the genetic model grass *Brachypodium distachyon*, we identified BdPOLAR, which forms a novel, distal polarity domain in SMCs that is reciprocal to the proximal PAN1 domain. Both polarity domains are required for the formative SC division yet exhibit distinct roles in regulating pre-mitotic nuclear migration and SMC division plane orientation, respectively. Nonetheless, the domains are linked as the proximal domain controls polarisation of the distal domain. In summary, we identified two opposing polarity domains that coordinate the SC division, a process crucial for grass stomatal physiology.

grass stomata I subsidiary cells I cell polarity I assymetric cell division I *Brachypodium distachyon* I stomatal gas exchange

Stomata are "breathing pores" in the plant epidermis that regulate gas exchange between the plant and the environment. They open to enable the entry of carbon dioxide to be assimilated in photosynthesis and close to restrict water vapour loss. Efficiently balancing carbon dioxide uptake and water vapour loss is key for plant survival and abiotic stress resilience. Grasses like *Zea mays* (maize), *Oryza sativa* (rice), and the genetic model system *Brachypodium distachyon* present a unique stomatal morphology, where a pair of central, dumbbell-shaped guard cells (GC) is flanked by two lateral subsidiary cells (SC) (Nunes et al., 2020; Stebbins and Shah, 1960). The grasses' stomatal morphology is linked to faster stomatal movements that contribute to more water-use efficient gas exchange (Franks and Farquhar, 2007; Lawson and Vialet-Chabrand, 2019; McAusland et al., 2016). Among other features, the grasses' morphological innovations to stomatal form and function likely contributed to their evolutionary success (Hetherington and Woodward, 2003) and their importance in modern agriculture (FAO Statistical Pocketbook, 2015).

The linear epidermal cell files in a growing grass leaf follow a stereotypic and strict developmental gradient from base to tip (Fig. 1A) (Stebbins and Shah, 1960). Some cell files acquire stomatal identity at the leaf base, where a transversal, asymmetric cell division (ACD) generates a small guard mother cell (GMC) and a large, interstomatal pavement cell precursor (Fig. 1A) (Raissig et al., 2016; Stebbins and Shah, 1960; Wu et al., 2019). The GMC then induces its lateral neighbour cells to become subsidiary mother cells (SMC), which strongly polarise towards the GMC and undergo an extreme longitudinal ACD to generate a proximal SC and a distal pavement cell (Fig. 1A) (Cartwright et al., 2009; Facette et al., 2015; Gray et al., 2020; Humphries et al., 2011; Nan et al., 2021; Raissig et al., 2017; Stebbins and Shah, 1960; Zhang et al., 2012). Finally, the GMCs undergo a symmetric longitudinal cell division generating two GC precursors before complex morphogenetic processes shape the so-called graminoid stomatal morphology (Fig. 1A) (Galatis and Apostolakos, 2004; Spiegelhalder and Raissig, 2021; Stebbins and Shah, 1960).

The lateral SCs represent one of two key morphological innovations of grass stomata (Gray et al., 2020; Nunes et al., 2020). It was shown that SC presence is critical for stomata to open and close quickly in response to environmental cues in grasses (Raissig et al., 2017) yet few factors required for SC formation have been identified. SC formation can be divided into three steps, (1) SMC establishment, (2) SMC polarization and (3) the ACD that yields the SC. Previous work showed that orthologs of the Arabidopsis stomatal bHLH transcription factor *MUTE* are required to establish SMC identity in the three grass species *B. distachyon*, maize and rice and that *mute* mutants lack SCs (Raissig et al., 2017; Wang et

al., 2019; Wu et al., 2019). In maize SMCs, a proximal polarity module localised at the GMC/SMC interface establishes pre-mitotic polarity and guides the migrating nucleus towards the GMC/SMC interface. ZmBRICK1 (ZmBRK1), a subunit of the SCAR/WAVE regulatory complex (WRC), initially localises at the interface of GMC/SMC (Facette et al., 2015). ZmBRK1 then promotes the polarized accumulation of two leucine-rich-repeat receptor-like kinases (LRR-RLKs) ZmPANGLOSS1 (ZmPAN1) and ZmPAN2 (Cartwright et al., 2009; Facette et al., 2015; Zhang et al., 2012). ZmPAN2 acts upstream of ZmPAN1, which then recruits two Rho of plants (ROP) GTPases, ZmROP2 and ZmROP9 (Humphries et al., 2011; Zhang et al., 2012). The ZmROPs physically interact with and possibly activate WRC components, which lead to actin patch formation at the GMC/SMC interface and nuclear migration (Facette et al., 2015). Upon nuclear migration, the phosphatases DISCORDIA1 (ZmDCD1) and ALTERNATIVE DCD1 (ZmACD1) control the formation and positioning of the preprophase band (PPB) (Wright et al., 2009), which is a transient cytoskeletal array that guides the future division plane (Facette et al., 2019; Livanos and Müller, 2019). After the disappearance of the PPB, factors such as the microtubule-binding protein TANGLED1 (TAN1) maintain the cortical division site (Cleary and Smith, 1998; Martinez et al., 2017). Finally, the myosin XI protein OPAQUE1 (O1)/DCD2 is critical for phragmoplast guidance during late cytokinesis and subsequent cell plate formation to complete the ACD that forms SCs (Nan et al., 2021).

In the Arabidopsis stomatal lineage, cell polarity and cytoskeleton-mediated nuclear migration and ACDs are regulated by a different set of polarity genes (Guo et al., 2021a; Muroyama and Bergmann, 2019; Ramalho et al., 2022). BREAKING OF ASYMMETRY IN THE STOMATAL LINEAGE (BASL), a dicot-specific protein, serves as an intrinsic polarity factor to regulate ACDs of meristemoid mother cells (MMCs) and forms a polarity crescent distal to the division plane (Dong et al., 2009). BASL promotes polarisation of BREVIS RADIX (BRX) family proteins and POLAR LOCALIZATION DURING ASYMMETRIC DIVISION AND REDISTRIBUTION (POLAR) within its own polarity domain (Pillitteri et al., 2011; Rowe et al., 2019). The Arabidopsis polarity proteins can scaffold kinases to regulate cell division capacity, fate asymmetry and nuclear migration (Guo et al., 2021a; Muroyama and Bergmann, 2019). POLAR recruits the glycogen synthase kinase 3 (GSK3)-like kinase BIN2 to regulate cell division capacity (Houbaert et al., 2018), whereas a positive-feedback loop between BASL and the mitogen-activated protein kinase (MAPK) pathway is essential for enforcing different cell fates after ACD (Zhang et al., 2015). BASL and its polarity domain also act to orient nuclear migrations during ACDs (Muroyama et al., 2020).

Here, we leveraged the unique *bdmute* phenotype to transcriptionally profile developing leaves that form SCs (wild-type) and leaves that lack SCs (*bdmute*). Among the genes

dependent on *BdMUTE* we identified the homolog of *AtPOLAR*, *BdPOLAR*, and showed it plays a role in SC formation. BdPOLAR not only occupied a distal polarity domain that is opposite of the proximal PAN1 polarity domain, but also BdPOLAR's polarisation was dependent on *BdPAN1*. Detailed and quantitative analysis of the *bdpan1* and *bdpolar* phenotypes suggested distinct roles in regulating pre-mitotic nuclear polarisation and division plane orientation, respectively.
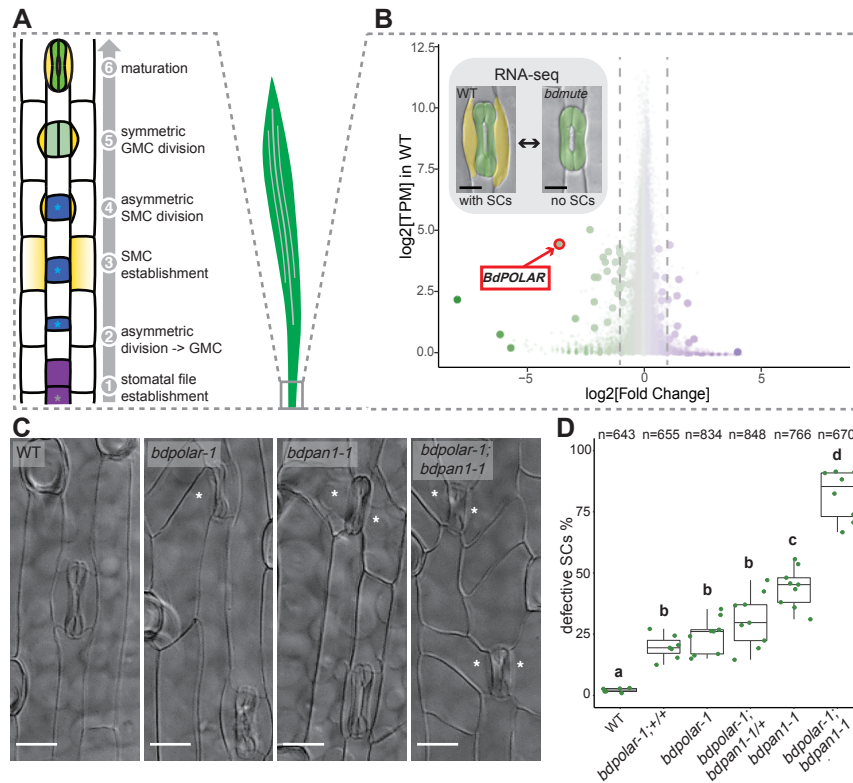
RESULTS

Comparative Transcriptomics Identify a Role for *BdPOLAR* in SC development

To identify novel factors regulating SC development in the grass stomatal lineage, we took advantage of the fact that loss of *MUTE* in *B. distachyon* did not result in seedling lethality. In rice and maize, *mute* mutants completely abort stomatal development and die, whereas *bdmute* plants are viable and form two-celled stomata that lack SCs (Raissig et al., 2017; Wang et al., 2019; Wu et al., 2019). We profiled the transcriptome of the developing *B. distachyon* leaf zone in wild-type (with SCs) and in *bdmute* (without SCs; Fig. 1B). Among the 35 downregulated genes in *bdmute* (Table S1), the fourth most downregulated gene was the homolog of Arabidopsis *POLAR* (At4g31805), a polarly localised protein of unknown function with a role in regulating ACDs in the Arabidopsis stomatal lineage (Houbaert et al., 2018; Pillitteri et al., 2011). To assess the functional relevance of *BdPOLAR* (BdiBd21-3.3G0715200 - Bradi3g54060), we induced targeted mutations at three different positions in the coding sequence using CRISPR/Cas9 (Fig. S1C, E, and F). The three alleles *bdpolar-1* (+T), *bdpolar-2* (+T) and *bdpolar-3* (+T) all failed to correctly divide 25-40% of their SCs (Fig. S1A, B). They showed oblique and misoriented SC division planes that resulted in missing or improperly formed SCs in mature leaf zones (Fig. 1C, D; Fig. S1A, B; Fig. S2A, B). These defects in asymmetrically dividing SMCs suggested that *BdPOLAR* played a role in regulating SMC polarisation and/or the formative SC division itself and that, unlike in *Arabidopsis (Houbaert et al., 2018)*, a single mutation affecting the *BdPOLAR* homolog severely affected grass stomatal development.

BdPOLAR and *BdPAN1* Are Both Required During the Formative SC Division

The *bdpolar* division defects were reminiscent of classical maize SMC polarity mutants like *zmpan1* and *zmpan2*, which caused incorrectly positioned, oblique ACDs in SMCs (Cartwright et al., 2009; Facette et al., 2015; Zhang et al., 2012). A *BdPAN1* mutant (BdiBd21-3.3G0526300 - Bradi3g39910, *bdpan1-1*) isolated in a screen for stomatal pattern defects contained a 9-base pair (bp) in-frame deletion near the 5'-end of *BdPAN1* and displayed ~45% aberrant and oblique SC divisions (Fig. 1C, D; Fig. S1D, F). This suggested that *bdpan1*

Figure 1. *BdPOLAR* is a novel regulator of SC division in the *B. distachyon* stomatal lineage. (A) Stomatal development in *B. distachyon*; in a stomatal file (1) (grey asterisk) a transverse asymmetric division (2) generates a GMC (blue, with blue asterisk), which laterally induces SMCs (yellow) (3). SMCs divide asymmetrically (4) before GMCs divide symmetrically (5) and the complex matures (6). **(B)** Volcano plot displaying wild-type expression level (y-axis) and fold change in *bdmute* compared to wild-type (x-axis) of all expressed genes in the developmental zone (dots = genes). Green, large dots indicate genes significantly downregulated in *bdmute* and purple, large dots indicate genes significantly upregulated in *bdmute*. The red circle indicates *BdPOLAR*. **(C)** Differential interference contrast (DIC) images of the epidermis in WT (Bd21-3), *bdpolar-1*, *bdpan1-1*, and *bdpolar-1; bdpan1-1* (third leaf, 19 days after germination (dag)). Aberrant SCs are indicated with white asterisks. Scale bar, 15 μm. **(D)** Quantifications of defective SCs of segregating lines after crossing (*bdpolar-1;+/+*, *bdpolar-1;bdpan1-1/+*, and *bdpolar-1;bdpan1-1*), the parental lines *bdpolar-1* and *bdpan1-1*, and a WT control. Samples were compared using a one-way ANOVA and posthoc Tukey test for multiple comparisons; different letters indicate significant differences (p<0.05). n=6-9 individuals and 643-848 SCs.

and *bdpolar* mutants caused similar phenotypes, albeit with different penetrance.

Examination of the developmental origins of defective SCs revealed that early transverse divisions generating GMCs were normal in both *bdpolar-1* and *bdpan1-1*. The longitudinal ACDs in SMCs, however, showed misoriented divisions. In both *bdpolar-1* and *bdpan1-1* some of the cell division planes were transverse rather than longitudinal (Fig. S2A, B, and C). This suggested that the origin of the aberrant SCs was incorrectly oriented ACDs during SC recruitment.

To explore the functional relationship between *BdPOLAR* and *BdPAN1*, we crossed the single mutants to generate the *bdpolar-1;bdpan1-1* double mutant. The double mutant displayed a much stronger phenotype with ~82% of abnormally divided SCs (Fig. 1C, D). Accordingly, the misoriented division planes in SMCs were overly abundant in *bdpolar-1;bdpan1-1* (Fig. S2D). This suggested that *BdPOLAR* and *BdPAN1* either work redundantly in the same cellular process or that they affect different elements of a complex pathway to properly orient and execute SMC divisions. However, none of the single mutants nor the double mutant showed any growth or fertility

defects in well-watered and optimized growth conditions.

The Polarity Domains of BdPOLAR and BdPAN1 Are Mutually Exclusive

The observed SMC division orientation phenotypes and the behaviour of *BdPAN1* and *BdPOLAR* homologs in other species suggested that these proteins might be polarly localised in GMCs and/or SMCs. A *BdPAN1p:BdPAN1-YFP* reporter line was expressed in all young protodermal cells and the protein was evenly distributed at the cell periphery (Fig. 2A; Fig. S3A). Once GMCs were formed and started to elongate (stage 3; Fig. 1A), BdPAN1 protein began to accumulate at the GMC/SMC interface (Fig. 2B, C; Fig. S3A). 3D imaging revealed that BdPAN1 formed a ring-like structure at the GMC/SMC interface (Fig. 2C; Video S1). Together, BdPAN1's expression and polarisation pattern were highly similar to the localization of *ZmPAN1* as observed by immunolocalization or translational reporter lines in *maize* (Cartwright et al., 2009; Sutimantanapi et al., 2014). In fact, all thus far identified regulators of SMC polarity (e.g. *ZmPAN1/2*, *ZmROP2/9* and *ZmBRK1*) polarised much like PAN1 towards the
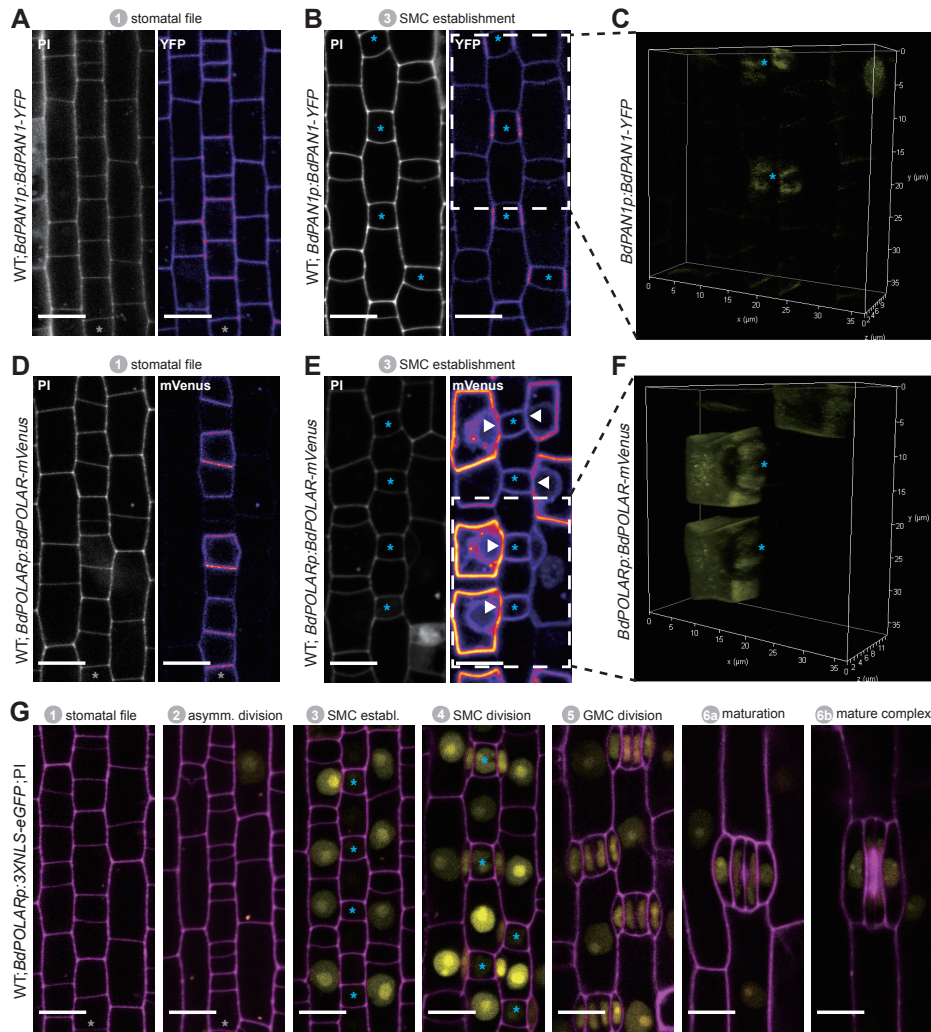
Figure 2. BdPAN1 and BdPOLAR display opposite, reciprocal polarisation in SMCs. (A, B) *BdPAN1p:BdPAN1-YFP* reporter expression in stage 1 stomatal files (A) and during SMC stage 3 (B). Images of PI-stained cell outlines (left), and fluorescence intensity of YFP channel (right). **(C)** 3D rendering of stage 3 field of view as indicated in (B); YFP channel only. **(D, E)** *BdPOLARp:BdPOLAR-mVenus* reporter expression in stage 1 stomatal files (D) and during SMC stage 3 (E). Images of PI-stained cell outlines (left), and fluorescence intensity of mVenus channel (right). The absence of *BdPOLAR* at the GMC/SMC interface is indicated with white arrowheads. **(F)** 3D renderings of stage 3 field of view as indicated in (E); mVenus channel only. **(G)** *BdPOLARp:3xNLS-eGFP* reporter expression during stomatal development. Overlay images show *BdPOLAR* transcriptional signals (in yellow) and PI-stained cell outlines in magenta. The stomatal files are indicated with grey asterisk. GMCs are indicated with blue asterisks. Developmental stages are indicated. Scale bar, 10 μm.

GMC/SMC interface (Facette et al., 2015; Humphries et al., 2011; Zhang et al., 2012).

Next, we generated a *BdPOLARp:BdPOLAR-mVenus* reporter line to analyse if BdPOLAR was also polarly localised in SMCs. Strikingly, signal was detected at the distal, the apical and the basal cell wall and was excluded from the classical polarity domain at the GMC/SMC interface. Thus, BdPOLAR defines a new, opposing polarised domain (Fig. 2E; Fig. S3B) in SMCs. In addition, unlike BdPAN1-YFP, which was initially expressed in all protodermal cells, *BdPOLAR* was only expressed in the stomatal lineage (Fig. 2D, Fig. S3B). Before SMCs were specified, weak BdPOLAR-mVenus signal appeared in the stomatal rows with a bias towards the base of stage 1 stomatal lineage cells and distal to the transverse asymmetric division generating GMCs (Fig. 2D; Fig. S3B). During stage 3 (SMC establishment, Fig. 1A) a strong and specific signal emerged in SMCs (Fig. 2E). Initially, the

signal appeared in the apical and basal plasma membrane (PM) of SMCs (Fig. S3B) before also occupying the distal PM (Fig. 2E). Just after the division, BdPOLAR quickly dissociated from the distal PMs (Fig. 2E; Fig. S3B). The signal then appeared in the GMCs, young GCs and young SCs but remained weak (Fig. S3B). The transcriptional *BdPOLAR* reporter (*BdPOLARp:3XNLS-eGFP*) showed *BdPOLAR* promoter activity first in SMCs, and only later in GMCs and expression was not detected in young stomatal cell files (Fig. 2G) suggesting that intronic elements may also contribute to BdPOLAR expression and accumulation.

Together, the analysis of translational SMC polarity reporter lines revealed a novel, distal polarity domain in SMCs that seemed to be reciprocally opposed to the well-established, proximal polarity domain at the GMC/SMC interface.
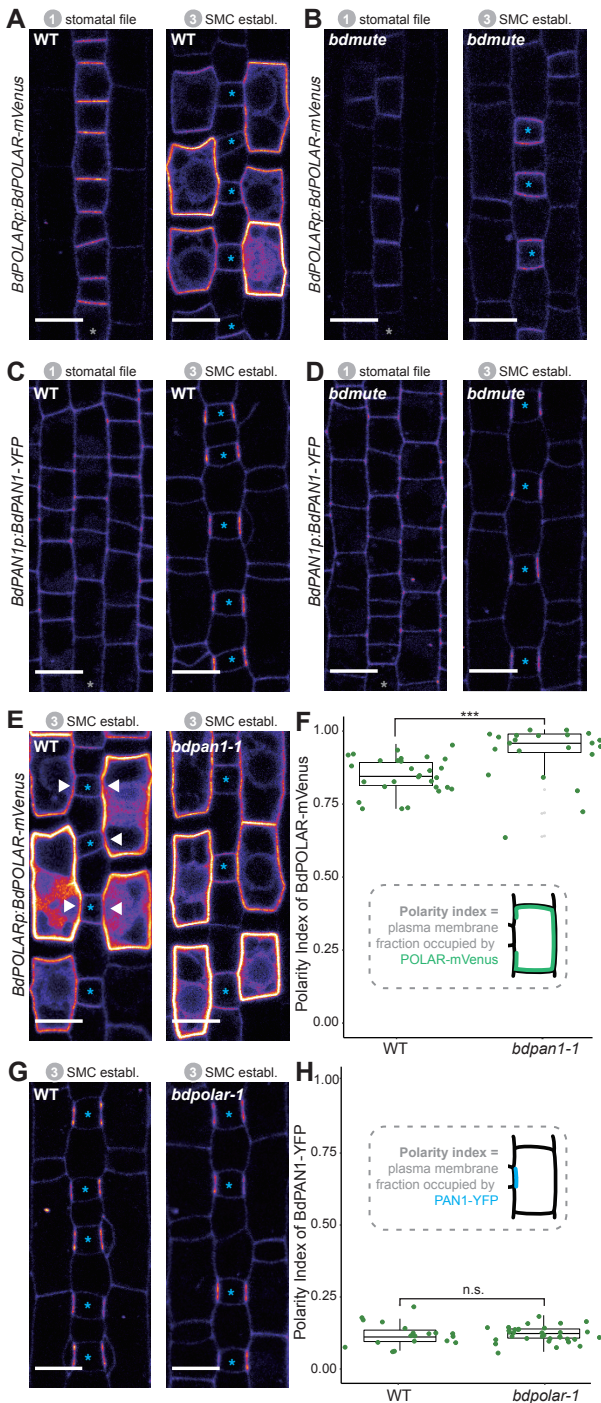
Figure 3. *BdPOLAR* expression requires *BdMUTE* and BdPOLAR polarization is controlled by *BdPAN1*. (A, B) Fluorescence intensity of *BdPOLARp:BdPOLAR-mVenus* in WT (A) and in *bdmute* (B) at stage 1 and stage 3. **(C, D)** Fluorescence intensity of *BdPAN1p:BdPAN1-YFP* in WT (C) and in *bdmute* (D) at stage 1 and stage 3. **(E)** Fluorescence intensity of *BdPOLARp:BdPOLAR-mVenus* in WT (left) and *bdpan1-1* (right) at stage 3. The absence of *BdPOLAR-mVenus* at GMC/SMC interfaces in WT is indicated with white arrowheads. **(F)** Quantification of the polarity index of *BdPOLAR-mVenus* in WT (n=29 SMCs) and *bdpan1-1* (n=22 SMCs). Insets represent that polarity index is the fraction of the PM occupied by the polarity protein. **(G)** Fluorescence intensity of *BdPAN1p:BdPAN1-YFP* in WT (left) and *bdpolar-1* (right) at stage 3. **(H)** Quantification of the polarity index of *BdPAN1-YFP* in WT (n=19 SMCs) and *bdpolar-1* (n=33 SMCs) Insets represent that polarity index is the fraction of the PM occupied by the polarity protein. Statistical difference was test with an unpaired Mann-Whitney U-test; *** = p-value < 0.001; n.s. = non-significant. The stomatal files are indicated with grey asterisks. GMCs are indicated with blue asterisks. Scale bar, 10 μm.

BdMUTE Is Required for *BdPOLAR* expression

BdPOLAR was 12-fold downregulated in *bdmute* compared to wild-type (Table S1). To confirm that *BdPOLAR* expression is dependent on *BdMUTE*, *BdPOLARp:BdPOLAR-mVenus* was introduced into *bdmute* through transformation. Because different transgenic lines were compared, we set up laser intensities so that the expression pattern in stage 1 stomatal files was comparable between *bdmute* and wild-type. In wild-type, we needed four times less laser to visualise BdPOLAR-mVenus signal in SMCs compared to the signal in stage 1 cell files (2% vs. 8%; Fig. 3A). In *bdmute*, however, we used twice as much laser for stage 3 SMCs than stage 1 stomatal cell files (20% vs. 38%) and still did not detect any signal in cells neighbouring the GMCs (Fig. 3B). Together with the comparative RNA-seq data, this suggested that *BdMUTE* was indeed required for *BdPOLAR* expression either directly through binding to the *BdPOLAR* promoter or indirectly through the establishment of SMCs and downstream programs.

In contrast, *BdPAN1p:BdPAN1-YFP* was expressed and properly polarised independently of *BdMUTE* (Fig. 3C, D). This observation suggested that BdPAN1 polarisation was independent of a successful establishment of the SC lineage in lateral cell files and indicated that either biochemical or mechanical signals from the elongating GMC polarise BdPAN1.

BdPAN1 Is Required for BdPOLAR Polarisation but not *Vice Versa*

In animal systems, opposing polarity domains can be mutually inhibitory (Muroyama and Bergmann, 2019; Ramalho et al., 2022; Nance and Zallen, 2011), yet such inhibitory relationships have not been identified in the plant kingdom. To test if the opposing BdPAN1 and BdPOLAR polarity domains showed an inhibitory relationship we crossed the BdPOLAR-mVenus and BdPAN1-YFP reporter lines to *bdpan1-1* and *bdpolar-1*, respectively. To quantify the degree of polarisation of BdPOLAR-mVenus and BdPAN1-YFP in wild-type and mutant SMCs, we employed Polarity Measurement (POME) to quantify the fraction of the plasma membrane occupied by the protein of interest and to determine the polarity index (Gong et al., 2021a, 2021b). In wild-type, the broad, distal BdPOLAR polarisation domain showed a much higher average polarity index (i.e. less polarised) than the highly polarised BdPAN1 domain at the GMC/SMC interface (Fig. 3F, H). In *bdpan1-1*, however, we observed an almost uniform distribution of BdPOLAR-mVenus signal at the periphery of SMCs, where BdPOLAR-mVenus seemed to have invaded the BdPAN1 domain at the GMC/SMC interface (Fig. 3E). Quantifying the polarity index of BdPOLAR-mVenus in *bdpan1-1* indeed showed a significantly decreased polarisation of BdPOLAR-mVenus (Fig. 3F). In contrast, BdPAN1-YFP polarised normally at the GMC/SMC interface independent of the presence or absence of functional BdPOLAR (Fig. 3G, H). Thus, functional BdPAN1

was required for polarised localization of BdPOLAR, but Bd-PAN1 localization was not affected in the *bdpolar-1* mutant background. This suggested that even though BdPAN1 and BdPOLAR show opposing polarisation patterns they exhibit a one-way rather than a mutual inhibition. This might be due to the earlier polarisation of BdPAN1, which accumulated at the GMC/SMC interface before BdPOLAR was expressed in SMCs (Fig. S3).

Accurate Dosage and Localization of BdPOLAR Is Necessary for Functionality

In addition to the non-polarised localization of Bd-POLAR-mVenus in *bdpan1-1*, the expression of BdPO-LAR-mVenus strongly exaggerated the *bdpan1-1* SC defect frequency (Fig. S4A). 86% of SMCs displayed abnormal formation in *bdpan1-1* plants that expressed BdPOLAR-mVenus compared to only ~30% in *bdpan1-1* plants without Bd-POLAR-mVenus expression (Fig. S4B). This suggested that having no BdPOLAR in *bdpan1-1* (i.e. the *bdpolar-1;bdpan1-1* double mutant) or too much and potentially mVenus-stabilised BdPOLAR in *bdpan1-1* had a similar deleterious effect on SC divisions. In fact, even wild-type plants with strong *BdPOLARp:BdPOLAR-mVenus* expression (~19%) or ubiquitously expressed BdPOLAR-mVenus (~10%) resulted in SC defects further indicating that correct dose and/or stability of Bd-POLAR seems to be crucial for its function (Fig. S4B, I, J).

Finally, only weak BdPOLAR-mVenus expression partially rescued *bdpolar-1* defects, while strong BdPOLAR-mVenus expression failed to complement altogether (Fig. S4C, D). It is also conceivable that the lines do complement but create a simultaneous, dosage-dependent overexpression phenotype. In contrast, we did not observe a dosage or stability effect of BdPAN1-YFP in wild type or *bdpolar-1,* and *BdPAN1p:BdPAN1-YFP* was able to fully complement the *bdpan1-1* mutant phenotype (Fig. S4E-H).

BdPAN1 Governs Nuclear Migration in Pre-mitotic SMCs to Orientate SMC Divisions

The phenotypes noticed in *bdpolar-1;bdpan1-1*, and the oppositely polarised domains of BdPOLAR and BdPAN1 suggested that *BdPOLAR* and *BdPAN1* act in parallel pathways and potentially execute different functions during SMC polarisation and division.

It was previously suggested that guiding pre-mitotic nuclear migration involved the ZmPAN1 polarity domain (Cartwright et al., 2009; Facette et al., 2015; Zhang et al., 2012). To test if *BdPAN1* is also required for pre-mitotic nuclear migration in *B. distachyo*n and to determine to what extent *Bd-POLAR* contributes to this process, we quantified the distance of the SMC nucleus to the GMC/SMC interface as a proxy for pre-mitotic SMC polarisation and nuclear migration (Fig. 4A). Images of developing wild-type leaf zones with stained

nuclei and cell outlines revealed that indeed most SMCs had polarised nuclei (Fig. 4B). In *bdpolar-1,* only a few SMCs displayed unpolarized nuclei (Fig. 4B), but in *bdpan1-1* and *bdpolar-1;bdpan1-1,* many SMCs showed unpolarized nuclei (Fig. 4B).

To accurately quantify the nuclear position as a function of the SMC's developmental stage, we not only measured the distance (d) from the nuclear centre to the middle of the GMC/SMC interface but also the length-to-width ratio (LWR) of the neighbouring GMC (Fig. 4A). SMC nuclei were located more proximal to the GMC/SMC interface next to longer and, thus, more mature GMCs (i.e. higher LWR of GMCs) (Fig. S5A). We chose a GMC LWR of 0.9 as cut-off since >93% of the SMC nuclei were within 4 μm of the GMC/SMC domain and thus considered polarised in wild type (Fig. S5C). In wild-type, the average distance of SMC nuclei to GMCs with an LWR >0.9 was 3.19 μm— the lowest distance value of all genotypes. The average distance of SMC nuclei was significantly increased in *bdpolar-1* (3.48 μm. Fig. 4C, Fig. S5C) but almost 80% of the nuclei were still within 4μm of the GMC/SMC interface. In *bdpan1-1* the average distance was clearly increased (3.78 μm. Fig. S5C) and more than 35% of the SMC nuclei were beyond the 4μm cut-off (Fig. 4C) suggesting that *BdPAN1* indeed affected nuclear migration more than *BdPOLAR*. Finally, the double mutant *bdpolar-1;bdpan1-1* displayed an almost identical nuclear migration defect (3.89 μm, and >37% unpolarized nuclei; Fig. S5C) as *bdpan1-1* single mutants (Fig. 4C). This suggested that nuclear migration defects in *bdpolar-1;bdpan1-1* were mostly caused by the loss-of-function of *BdPAN1*, and indicated that nuclear migration is dominated by BdPAN1 rather than Bd-POLAR activity (Fig. 4C). In addition, the fraction of unpolarized SMC nuclei in *bdpan1-1* and the *bdpolar-1;bdpan1-1* mutants are similar, yet the defective SMC divisions are twice as frequent in the double mutant. This suggested that the exaggerated ACD defects in the double mutant might not solely be induced by deficient nuclear migration.

BdPOLAR Regulates Cortical Division Site Orientation and Cell Division Potential

As defective nuclear migration cannot explain the severe SC division defects in *bdpolar-1;bdpan1-1*, another, yet unknown pathway must also be affected and likely involves *Bd-POLAR*. We not only found an absence of BdPOLAR-mVenus signal at the GMC/SMC interface but also at the cortical division sites just above and below the GMC/SMC interface, which was visible both in 2D images (Fig. 2E) and 3D images of BdPOLAR-mVenus localization in SMCs (Fig. 2F; Video S2). We, therefore, hypothesised that *BdPOLAR* might have a role in specifying cortical division sites and cell division orientation. To test this possibility, we generated *BdTAN-GLED1-mCitrine* reporter lines specifically expressed in dividing SMCs and GMCs (using the *BdPOLAR* promoter), which stably marked cortical division sites throughout mitosis (Fig.
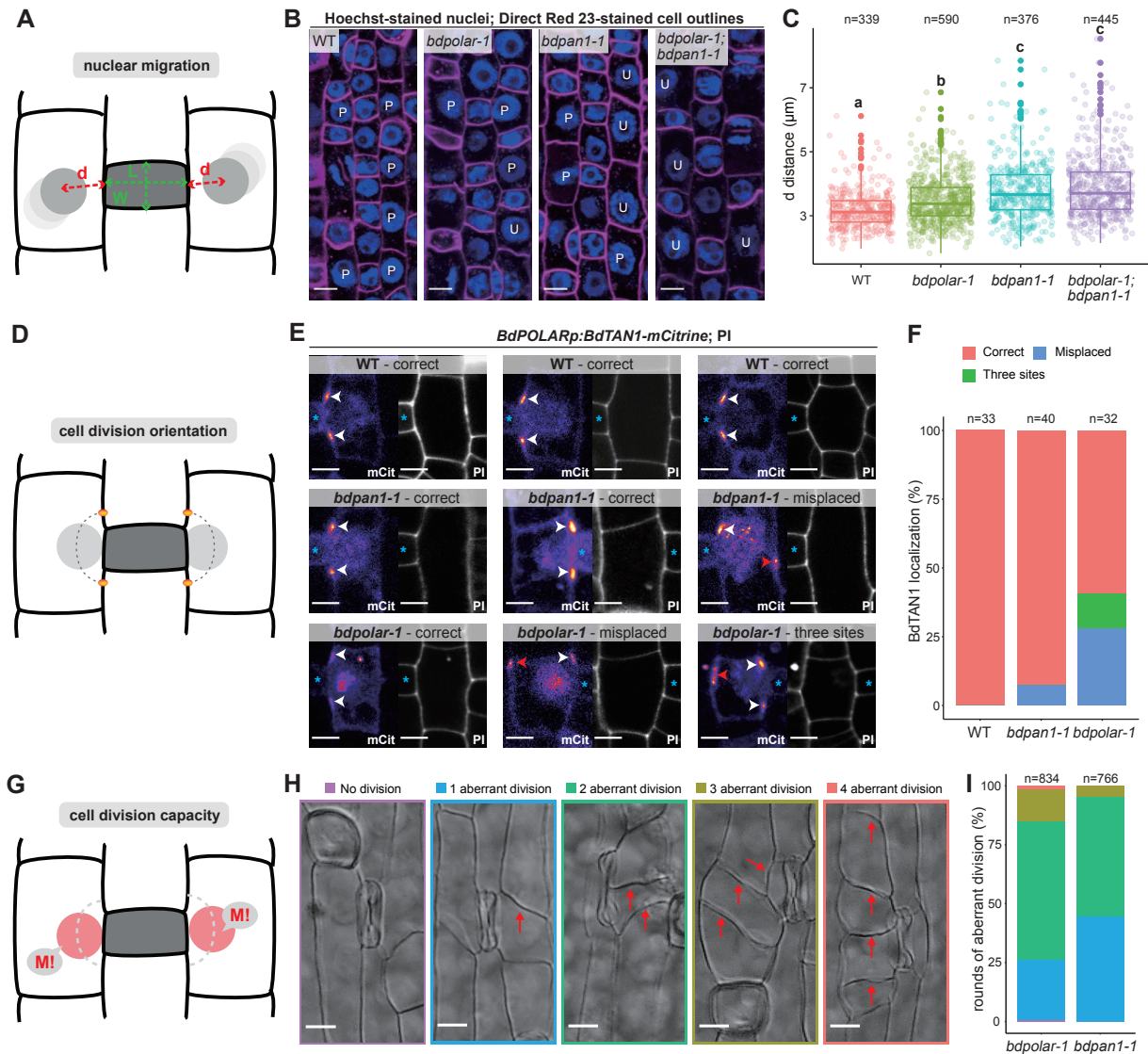
Figure 4. BdPAN1 controls nuclear migration and BdPOLAR controls cortical cell division orientation and division capacity in SMCs. (A) Schematic of the quantification of nuclear migration. L: GMC length; W: GMC width; d: the distance between the nuclear centre to the middle of the GMC/SMC interface. **(B)** Single confocal plane images of Hoechst-stained nuclei and Direct Red 23-stained cell outlines of stage 3 to stage 4 SMCs in WT, *bdpolar-1*, *bdpan1-1*, and *bdpolar-1;bdpan1-1*; P, polarized nucleus; U, unpolarized nucleus. Scale bar, 10 µm. **(C)** Quantification of d in SMCs of WT, *bdpolar-1*, *bdpan1-1*, and *bdpolar-1;bdpan1-1*; only SMCs flanking GMCs with a LWR>0.9 are shown. Numbers of SMCs measured are indicated. Samples were compared using a one-way ANOVA and post-hoc Tukey test for multiple comparisons; different letters indicate significant differences ($p<0.05$). **(D)** Schematic showing future division plane and expected BdTAN1 localization (orange) at the cortical division site. **(E)** *BdPOLARp:BdTAN1-mCitrine* expressed in WT, *bdpan1-1,* and *bdpolar-1*; three different SMCs are shown per genotype. Correct BdTAN1-mCitrine localization is indicated with white arrowheads; misplaced cortical division sites are indicated with red arrowheads. Note that BdTAN1-mCitrine signal is also present in SMC nuclei and nucleoli. GMCs are indicated with blue asterisks. Scale bar, 5 µm. **(F)** Percentages of correct, misplaced, and three cortical division sites in WT, *bdpolar-1* and *bdpan1-1*; the numbers of SMCs analysed are indicated. **(G)** Diagram indicating SMC division potential (M!). **(H)** DIC images of different SMC division frequencies observed in the mature leaf epidermis of *bdpolar-1;bdpan1-1*; No division (purple), 1 aberrant division (blue), 2 aberrant divisions (green), 3 aberrant divisions (olive); 4 aberrant division (red). The division planes are indicated with red arrows. Scale bar, 10 µm. **(I)** Percentages of different SMC division categories in *bdpolar-1* and *bdpan1-1*; numbers of SMCs analysed are indicated.

4E) much like its maize homolog (Martinez et al., 2017). In B. distachyon, however, BdTAN1-mCitrine also shows weak expression in the nucleus and nucleolus (Fig. 4E). In wild-type SMCs, BdTAN1 has always localised above and below the GMC/SMC interface, correctly predicting the future SC division plane (100%, n=33; Fig. 4E, F). In *bdpan1-1* SMCs, BdTAN1 is still mostly localised to the "wild-type"-like proximal division site independent of nuclear polarisation (92.5%, n=40; Fig. 4E, F). In *bdpolar-1* SMCs, however, we found

that in 28.1% of cases (n=32) BdTAN1 is mis-localised to the proximal and distal PM predicting a transverse, oblique rather than longitudinal, curved division plane. In addition, in 12.5% of *bdpolar-1* SMCs, BdTAN1 marked three rather than just two cortical sites (Fig. 4E, F). This indeed suggested a role for *BdPOLAR* in orienting cell division planes in SMCs.

In addition, two lines of evidence suggested an additional role of *BdPOLAR* in regulating cell division potential (Fig.
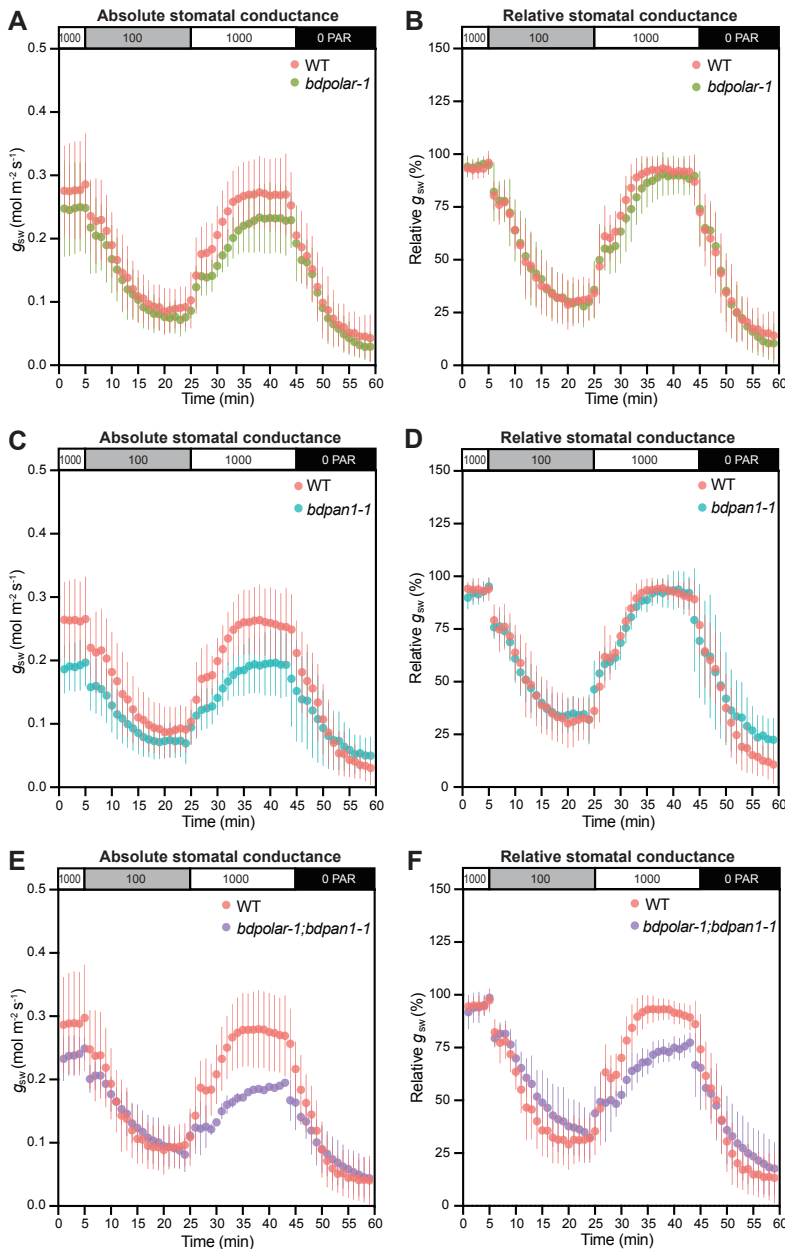
Figure 5. Wrongly divided SCs affect stomatal gas exchange levels and kinetics. (A, C, and E) Absolute stomatal conductance (g_{sw}) in response to light transitions (1000 PAR - 100 PAR - 1000 PAR - 0 PAR) in *bdpolar-1* (A), *bdpan1-1* (C), and *bdpolar-1; bdpan1-1* (E) compared to paired WT measurements. **(B, D, and F)** Relative stomatal conductance (g_{sw} normalized to highest g_{sw} observed) in response to light transitions (1000 PAR - 100 PAR - 1000 PAR - 0 PAR) in *bdpolar-1* (B), *bdpan1-1* (D), and *bdpolar-1; bdpan1-1* (F) compared to paired WT measurements. n=5 individuals per mutant genotype and 7 WT individuals. Error bars represent standard deviation.

4G). First, we realised that individual SMCs in both *bdpolar-1* and *bdpan1-1* can undergo more than one round of misoriented ACDs (Fig. 4H), thus, we counted the number of cell divisions per individual SMC in both mutant backgrounds. Indeed, in *bdpolar-1* almost 75% of the SMCs divided more than one time, whereas only 55% of the SMCs in *bdpan1-1* divided more than once (Fig. 4H, I). In *bdpolar-1*, we even observed a small fraction of SMCs (1.5%) that exhibited four rounds of aberrant cell division, which we never saw in *bdpan1-1* (Fig. 4H, I). On average, SMCs divided 1.9 times in *bdpolar-1* but only 1.6 times in *bdpan1-1*.

Also, successful recruitment of wild-type-like SCs seemed to occur at later stages in *bdpolar-1* compared to *bdpan1-1*. We thus quantified the LWR of GMCs that successfully recruited one or two wild-type-like SCs as a proxy for developmental stage/maturity in wild type, *bdpan1-1*, *bdpolar-1* and *bdpolar-1;bdpan1-1* (Fig. S6A, C). We found that the LWR of GMCs that recruited one or two SCs was always higher in *bdpolar-1* and *bdpolar-1;bdpan1-1* compared to *bdpan1-1* and

wild type (Fig. S6B, D). This suggested that GMCs that successfully recruited SCs were developmentally more mature in *bdpolar-1* and *bdpolar1;bdpan1-1* compared to *bdpan1-1* and wild type. This could be due to a potential developmental delay in *bdpolar-1*, or more likely in the light of the higher division potential of *bdpolar-1* SMCs (Fig. 4I) reflecting that more rounds of divisions occured until successful SC recruitment was completed. Together, these findings suggested that *BdPOLAR* might not only have a role in regulating cell division orientation in SMCs but could also affect their cell division potential.

Morphologically Aberrant SCs Negatively Impact Stomatal Gas Exchange

We have previously shown that *bdmute* stomatal complexes that failed to specify and recruit SCs altogether displayed severely impaired stomatal dynamics and gas exchange capacity (Raissig et al., 2017). In *bdpolar-1;bdpan1-1* double mutants

also ~82% of SCs fail to form correctly (Fig. 1D). Yet in *bd-polar-1;bdpan1-1*, the neighbouring cells presumably adopted SC lineage identity through the action of *BdMUTE* but failed to properly divide and form SCs. To test opening and closing speediness, we performed gas exchange measurements in a changing light regime. We found that both single mutants and the double mutant *bdpolar-1;bdpan1-1* showed lower absolute stomatal conductance (g_{sw}; Fig. 5A, C, and E; Table S3) that seemed proportional to the number of aberrantly formed SCs (Table S3). This was not linked to reduced stomatal density (Fig. S7A) but rather stomatal size (Fig. S7B), as GCs without SCs tend to be shorter and accordingly have shorter pores (Nunes et al., 2022). In contrast, the analysis of relative g_{sw} (values normalised to maximum stomatal conductance per genotype and individual), which visualises differences in stomatal opening and closing kinetics, showed slower stomatal movements in the double mutant only (Fig. 5B, D, and F; Fig. S7C, D, and E). This indicated that a majority of SCs must be defective to affect speed. In addition, the effect on speediness seemed less severe in *bdpolar-1;bdpan1-1* compared to *bd-mute* (Raissig et al., 2017) suggesting that the mis-divided cells flanking the GCs in *bdpolar-1;bdpan1-1* might retain residual SC functionality.

DISCUSSION

In this study, we identified *BdPOLAR* as a new, stomatal lineage-specific polarity factor that is required for the formative cell division that yields the functionally highly relevant stomatal SCs in the model grass *B. distachyon*. Strikingly, *Bd-POLAR* defined a new, distal polarity domain that was reciprocal to the proximal BdPAN1 polarity domain at the GMC/SMC interface (Fig. 6A). The BdPOLAR domain seemed functionally distinct from the BdPAN1 domain, yet BdPO-LAR's polarised localization was tightly linked to BdPAN1 (Fig. 6B).

In *Arabidopsis*, POLAR, like the BRX family and BASL, polarises distal to the nascent division plane, with BASL acting as a landmark for pre-mitotic nuclear migration away from the domain (Muroyama et al., 2020). In grasses, however, the positional cue for nuclear migration seems to be linked to the PAN1 polarity domain at the GMC/SMC interface, which is proximal to the division plane and is required to attract rather than repel the migrating SMC nucleus pre-mitotically (Fig. 6B) (Cartwright et al., 2009; Facette et al., 2015; Humphries et al., 2011). In *B. distachyon*, the PAN1 polarity domain is formed independently of SMC identity (i.e. also in *bdmute*) and, thus, seems to be primarily following mechanical or biochemical signals from the rapidly elongating GMCs (Giannoutsou et al., 2016; Livanos et al., 2015, 2016; Nunes et al., 2020). Furthermore, the PAN1 polarity domain is established significantly before the SMC division and persists significantly after the SMC division until late stages. This sug-
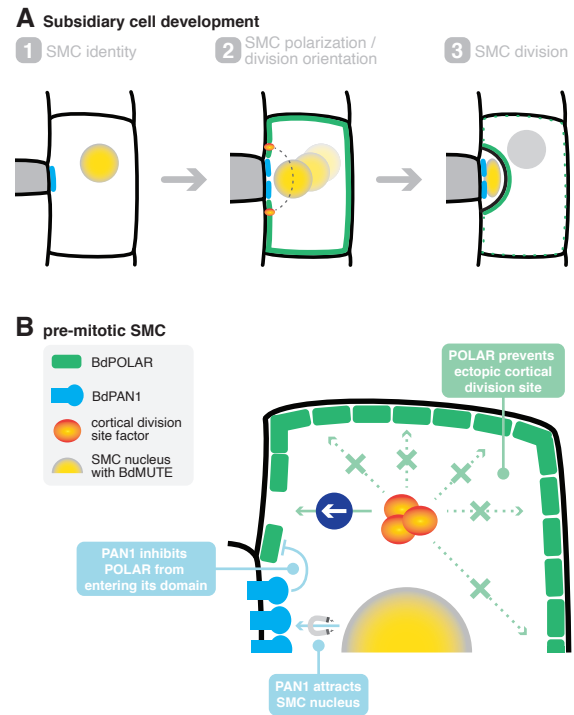
Figure 6. A mechanistic model of SMC polarisation by the two oppositely polarised BdPOLAR and BdPAN1 domain. (A) Stages of SC development. (1) SMC identity is established by *BdMUTE* and BdPAN1 polarises at the GMC/SMC interface independent of SMC establishment. (2) BdPOLAR is strongly expressed in SMCs and localizes at the apical, basal and distal PM of SMCs and is excluded from the BdPAN1 domain. The SMC nucleus migrates towards the GMC/SMC interface and the cortical division sites are established above and below the GMC/SMC interface. (3) An asymmetric cell division generates a smaller SC and a larger pavement cell. BdPOLAR quickly dissociates from the PM and reorients towards the newly formed plasma membrane. **(B)** Cellular mechanisms of BdPAN1 and BdPOLAR in pre-mitotic SMCs. BdPAN1 guides the migration of the SMC nucleus towards its own domain. BdPAN1 actively inhibits BdPOLAR from entering its domain, either biochemically or by steric hindrance. Distal BdPOLAR prevents cortical division site factors from ectopically binding and forces it to form specifically where BdPO-LAR protein level is low.

gests that the PAN1 domain is a "primary" polarity domain that reads SC lineage independent polarity cues and is stably positioned at the GMC/SMC interface throughout stomatal development. Finally, BdPAN1 is initially expressed in all protodermal cells and only later executes an SC-specific, polarised accumulation.

BdPOLAR, on the other hand, is specifically expressed in the stomatal lineage. Its expression is strongest in SMCs, which depends on *BdMUTE* establishing SC identity. This suggests that unlike the PAN1 domain, which seems to respond to intercellular polarization cues, BdPOLAR might be a cell-autonomous polarity factor linked to a specific cell fate. In addition, BdPOLAR is the first SMC polarity factor that forms a polarity domain distal to the future division plane in SMCs. BdPOLAR shows strong but transient polarised localization before it is quickly dissociated from the PM after completion of the ACD (Fig. 6A, B). The transient nature of BdPOLAR localisation might underlie its sensitivity to

dosage and/or altered protein stability potentially explaining the incomplete rescue of the *bdpolar* phenotype by the translational reporter. Similarly, YFP-ZmROP2 reporter lines in maize showed SCs defects likely due to dosage and mislocalisation effects of YFP-ZmROP2 in SMCs (Humphries et al., 2011). Much like for BdPOLAR-mVenus, YFP-ZmROP2 expression levels and SC division defects were correlated (Humphries et al., 2011).

Strikingly, the distally polarised localization of BdPOLAR depends on BdPAN1 (Fig. 6B) and in the absence of a functional BdPAN1 domain, BdPOLAR was able to invade the GMC/SMC interface. This suggests that the BdPAN1 domain either sterically hinders BdPOLAR from entering the GMC/SMC interface by prior occupation of this domain or it induces localised degradation of BdPOLAR through protein modification. This supports a hierarchical model, where a cell-fate independent polarity domain (BdPAN1) polarizes a cell-fate dependent polarity domain (BdPOLAR). Finally, much like the PAN homologs, BdPOLAR then persists in young GCs and SCs. While ZmPAN2 was shown to have a role in SC morphogenesis (Sutimantanapi et al., 2014), there is no obvious role for the grass PAN1 homologs or BdPOLAR in the SC lineage after the SC division. A role for BdPAN1 and BdPOLAR in the GC lineage is difficult to assess because absence of SCs affected GC length and morphology (Raissig et al., 2017).

In *B. distachyon*, *BdPOLAR* was initially expressed in the GC lineage and seemed to polarise to the base of dividing cells likely following similar polarity cues as *AtBASL* when it was ectopically expressed in *B. distachyon* (Nir et al., 2022). Functionally, however, BdPOLAR played no role in this first ACD that generated the GMC. Upon *BdMUTE*-dependent specification of SMCs, BdPOLAR is redeployed from the GC to the SC lineage, where it is functionally required during ACD. The absence of BdPOLAR signal at cortical division sites and cortical division site mislocalisation revealed by *BdTAN1* reporter imaging in *bdpolar-1* suggested a role in placing and orienting the cortical division site (Fig. 6B). The rather uniquely positioned cortical division sites in SMCs and strikingly curved SC wall (Fig. 6A) might underlie the requirement for not only one but two polarity domains, one of which is cell fate-specific and orients this peculiar division. The mechanism by which *BdPOLAR* affects division plane orientation is yet to be determined. We propose that the BdPOLAR domain actively repels microtubules or cortical division site factors like DCD1 and ACD1 (Wright et al., 2009) and/or PHRAGMOPLAST ORIENTING KINASES (POKs) (Herrmann et al., 2018; Lipka et al., 2014; Müller et al., 2006) (Fig. 6B). Temporally, however, it seems to act before cell plate formation and phragmoplast expansion and guidance, which is controlled by OPAQUE1/DISCORDIA2 in SMCs (Nan et al., 2021).

In addition to *BdPOLAR*'s role in cell division orientation, it also affected cell division capacity. In Arabidopsis,

AtPOLAR interacts and sequesters the GSK3-like kinase BIN2 that prohibits it from inhibiting the transcription factor SPEECHLESS (SPCH) (Houbaert et al., 2018), which establishes stomatal identity and regulates stomatal ACDs (MacAlister et al., 2007). Right at the onset of mitosis, a BSL family phosphatase is recruited to the polarity crescent in meristemoids, which releases BIN2 (Guo et al., 2021b). This enables BIN2 to enter the nucleus, downregulate SPCH and inhibit ACD potential in the larger daughter cell (Guo et al., 2021b; Houbaert et al., 2018). Accordingly, mutants affecting several POLAR family members in Arabidopsis show reduced cell division capacity in meristemoids. In grasses, a mutation in *BdPOLAR* alone was sufficient to reveal the family's functional relevance, yet *bdpolar* SMCs exhibited an increased rather than a decreased cell division capacity. Whether this reversed functionality also involves the sequestration of signalling components that directly or indirectly affect the cell cycle or is just a consequence of misoriented division planes remains elusive. It is possible, for example, that properly migrated SMC nuclei at the GMC/SMC interface in *bdpolar* but not in *bdpan1* might positively affect cell division capacity.

SCs functionally contribute to the fast opening and closing kinetics of grass stomata by acting as water and ions reservoirs and by providing mechanical support to GC movement through inverse turgor regulation (Franks and Farquhar, 2007; Gray et al., 2020; Nunes et al., 2020). Compared to *bdmute* plants, where the SC lineage is never established, *bdpolar-1;bdpan1-1* showed an overall milder defect in respect to opening and closing speediness (Raissig et al., 2017). This could be due to fewer SCs being defective in *bdpolar-1;bdpan1-1* (82%) compared to *bdmute* (almost 100%), which also results in a reduced effect on GC size and shape. Also, *bdmute* shows lower stomatal density (~30% of stomata abort), which is correlated with slower stomatal kinetics in *B. distachyon* (Nunes et al., 2022). Alternatively, and unlike in *bdmute*, wrongly divided SCs in *bdpolar-1;bdpan1-1* might have acquired and retained residual SC identity thus expressing appropriate ion channels, signalling modules or cell wall modifiers, which could positively influence stomatal kinetics. If partial SC-like functionality did not require anatomical changes to the stomatal complex, then stomatal speediness could be more easily engineered in crops that form stomata without SCs.

In conclusion, we identified a novel, cell fate-dependent, distal polarity domain that is polarized by a SC lineage-independent, proximal polarity domain. Apparently, the peculiar, highly asymmetric division of SMCs seems to require two connected, yet functionally distinct polarity domains to faithfully form this highly relevant cell type for efficient gas exchange in grasses.

AUTHOR CONTRIBUTIONS

Conceptualization, D.C.B. and M.T.R.; Investigation, D.Z., E.A., T.D.G.N. I.H.P., M.X.A.G, B.J., H.L., M.T.R.; Writing – Original Draft, D.Z., H.L., M.T.R.; Writing – Review & Editing, all authors; Supervision, H.L., D.C.B., M.T.R.; Funding Acquisition, D.C.B. and M.T.R.; Project Administration, H.L., D.C.B., M.T.R.

DECLARATION OF INTERESTS

The authors declare no competing interests.

MATERIAL AND METHODS

Transcriptional profiling of WT and SC-less leaves by RNA-sequencing

Approximately 3 cm long 2nd leaves of wild-type (Bd21-3) and *sid/bdmute-1* seedlings (7 days after germination grown on ½ MS plates at 20°C with ~100 μmol photons m^{-2} s^{-1} light) were carefully pulled out of the sheath of the 1st leaf to isolate the leaf developmental zone (3mm at base of the leaf). 25 developmental zones were collected per replicate and genotype (3 replicates per genotype), snap-frozen in liquid nitrogen and ground using mortar and pistil. Total RNA was isolated using Qiagen's RNeasy Plant Mini kit with on-column DNAse digestion according to the manufacturer's instructions. The Kapa mRNA HyperPrep (Roche) was used to generate an mRNA enriched sequencing library with an input of 1μg of total RNA. The libraries were sequenced using the Illumina NextSeq500 platform. Read quality was assessed with FastQC and mapped against the Bd21-3v1.0 genome using bowtie2. Mapped reads were counted using summarised overlap and differentially expressed genes were analysed using DeSeq2 (Love et al., 2014). Finally, gene expression was normalised by transcripts per kilobase million (TPM). Raw and processed data are available at Gene Expression Omnibus (GEO) with the accession number GSE201294.

Plant Material and Growth Conditions

Brachypodium distachyon Bd21-3 was used as wild-type. For plate-based seedling growth, seeds of Bd21-3, mutants and reporter lines were sterilised for 15min in 20% bleach (Carl Roth) and 0.1% Triton-100 (Carl Roth), thoroughly rinsed and placed on MS plates (½ MS (Duchefa Biochemie), 1% Sucrose (w/v, Carl Roth), 1% Bacto Agar (w/v, BD), pH 6). The seeds on plates were then stratified and vernalized for at least 2 days at 4 °C before transfer to a 28 °C chamber with 16h light:8h dark cycle (110 μmol PAR m^{-2} s^{-1}. Plants that were directly transferred to soil, were dehusked, vernalized and stratified in water for at least 2d at 4°C and then directly transferred to pots filled with soil, consisting of 4 parts ED CL73 (Einheitserde) and 1 part Vermiculite and grown in a greenhouse with 18h light:6h dark cycle (250-350 μmol PAR m^{-2} s^{-1}; day temperature = 28°C, night temperature = 22°C); see also (Haas and Raissig, 2020).

The three *bdpolar* mutant alleles (*bdpolar-1*, *bdpolar-2*, *bdpolar-3*) used for this study were generated by CRISPR/Cas9-based gene editing. The *bdpan1-1* mutant allele was isolated in a forward genetic screen of ethyl methanesulfonate mutagenized Bd21-3 seeds kindly provided by J. P. Vogel (DOE-JGI). All reporter lines in this study were specifically generated (see below).

Generation of CRISPR/Cas9 lines

Two CRISPR/Cas9 systems were used; the *bdpolar-1* allele was created following the design protocol of (Miao et al., 2013), while *bdpolar-2* and *bdpolar-3* were generated using the vectors and protocols of (Debernardi et al., 2020). We used CRISPR-P 2.0 (http://crispr.hzau.edu.cn/cgi-bin/CRISPR2/CRISPR) to select candidate guide RNA spacer sequences and chose suitable guides with a high on-score (few off-score hits). To generate *bdpolar-1*, double-stranded spacer sequences were generated by hybridising the oligo duplexes BdPOLAR-gRNA3-FWD+REV (priMR343 and priMR344) for CRISPR BdPOLAR-gRNA-3 and ligated into the BsaI-HF digested and dephosphorylated pOs-sgRNA vector (Miao et al., 2013). Entry clones were then introduced into the destination vector pH-Ubi-Cas9-7 which also encodes the Cas9-enzyme (Miao et al., 2013) using LR recombination (Invitrogen). T1 CRISPR/Cas9 lines were genotyped for the absence of the T-DNA construct by using the primers priMR410/411 (Hyg-1F/Hyg-1R). Genotyping of *bdpolar-1* was performed by amplifying the mutated region using priDZ6 and priDZ83 followed by Sanger sequencing of the amplicon. In addition, we designed a CAPS assay for the same amplicon using the BseRI restriction enzyme (Thermofisher); *bdpolar-1* has a +T insertion, which creates a BseRI restriction site in the mutant allele and only the mutant allele is cut after digestion (Fig. S1E). The *bdpolar-2* and *bdpolar-3* alleles were generated using the protocol from (Debernardi et al., 2020). Oligo duplexes of *BdPOLAR* guide 2 (priDZ87 and priDZ133 for *bdpolar-2* target site) and guide 4 (priDZ89 and priDZ134 for *bdpolar-3* target site) were hybridised and phosphorylated. Then the oligo duplexes were ligated into the AarI-digested (Thermofisher) destination vector JD633_CRISPRhigheff that encodes for a ubiquitously expressed Cas9 enzyme and regeneration enhancing chimeric GRF–GIF1 protein. To identify the edited mutation a 665 bp fragment was amplified using priDZ6/priDZ7 including all three target sites of the designed gRNAs and Sanger sequenced.

All primer sequences can be found in Table S2.

Generation of Reporter Constructs.

Most expression constructs in this study were generated based on the GreenGate system (Lampropoulos et al., 2013). Only the *BdPAN1* translational reporter construct was built using the Gateway-compatible pIPKb monocot vector series (Himmelbach et al., 2007), and the cortical division site marker *BdTAN1* reporter construct was produced via Gibson Assembly.

For GreenGate cloning, we first generated entry modules (pGGA-F). Inserts were amplified with Q5 DNA Polymerase (New England Biolabs) from *Brachypodium* Bd21-3 genomic DNA extracted using the DNeasy Plant Mini Kit (Qiagen) or specific plasmids using primers that contained Type IIS restriction sites and overhangs complementary to the respective entry module. The amplicons were then digested with FastDigest Eco31I (Thermofisher) to reveal the complementary overhangs. Simultaneously the corresponding backbone (pGGA000 for promoter, pGGC000 for coding sequence, pGGF000 for resistance cassette) was digested using Eco31I and dephosphorylated using antarctic phosphatase (Thermofisher). Then the amplicon was ligated into the backbone using T4 DNA ligase (Thermofisher). All built entry modules were analysed by test digestions and the inserted fragments were completely Sanger sequenced before proceeding.

BdPOLAR reporter constructs: To produce the entry module pGGA_BdPOLARpro, the 1137 bp intergenic region upstream of *BdPOLAR* was amplified using priDZ2/priDZ30 and ligated into the pGGA backbone. To clone the *BdPOLAR* genomic ORF without STOP into pGGC000, priDZ31 and priDZ35 were designed to mutate and remove the Eco31I site located in the first intron. priDZ3/35 and priDZ31/5 were used to amplify two fragments from Bd21-3 genomic DNA separately, then these two inserts were digested and ligated into digested and dephosphorylated pGGC000 to generate pGGC_BdPOLAR-NS. pGGF_PvUbi2pro-HygR entry module was cloned using switchgrass (*Panicum virgatum*) *ubiquitin 2* (*PvUbi2*) promoter driving hygromycin (Hyg) expression and the fragment was amplified from pTRANS_250d (Čermák et al., 2017). priTN11/priNT30 and priTN12/29 were used to amplify two fragments from pTRANS_250d plasmid separately, then these two inserts were digested and ligated into digested and dephosphorylated pGGF000 to generate pGGF_PvUbi2pro-HygR. To produce the entry module pGGA_ZmUbipro, *ZmUbi* promoter was amplified from pIPK002 (Himmelbach et al., 2007) using priTN3/4 and ligated into pGGA000. To generate *BdPOLARp:BdPOLAR-mVenus* expression vector, pGGA_BdPOLARpro, pGGB003 (dummy), pGGC_BdPOLAR-NS, pGGD_linker-mVenus, pGGE001 and pGGF_PvUbi2pro-HygR were introduced into the destination vector pGGZ004 by GreenGate reaction. GreenGate reaction enables the orderly assembly of six entry vectors into the destination vector by a set of seven different overhangs (Lampropoulos et al., 2013). It was performed by mixing 1.5 µl of each of the six modules, 1 µl destination vector, 2 µl FastDigest buffer (Thermofisher), 2 µl ATP (10 mM, Thermofisher), 0.5 µl T4 DNA ligase (30 u/µl, Thermofisher), 0.5 µl Eco31I and 5 µl H_2O in a total volume of 20 µl, then incubated for 50 cycles of 37ºC for 5 minutes and 16ºC for 5 minutes each, followed by 50ºC for 5 minutes and 80ºC for 5 minutes. The products of the GreenGate reactions were analysed by test digestions and sequencing of the ligation sites. To clone the expression vector for transcriptional reporter *BdPOLARp:3XNLS-eGFP*, pGGA_BdPOLARpro, pGGB_3xNLS, pGGC_eGFP, pGGD002 (dummy), pGGE001 and pGGF_PvUbi2pro-HygR were assembled into pGGZ004 by GreenGate reaction. To generate C-terminal tagged overexpression *ZmUbip:BdPOLAR-mVenus* reporter, pGGA_ZmUbipro, pGGB003, pGGC_BdPOLAR-NS, pGGD_linker-mVenus, pGGE001 and pGGF_PvUbi-

2pro-HygR were introduced into pGGZ004 by GreenGate reaction.

The generation of the entry modules pGGA000, pGGB003, pGGC000, pGGD002, pGGE001, and pGGF000 are described in (Lampropoulos et al., 2013). The entry modules pGGD_linker-mVenus are described in (Waadt et al., 2020), and pGGZ004 is described in (Lupanga et al., 2020). The pGGB_3xNLS and pGGC_eGFP were generously provided by Karin Schumacher's group. The pGGD009 (Linker-mCitrine) was generously provided by Jan Lohmann's group.

BdPAN1 translational reporter construct: First, the Bd-PAN1 genomic sequence was amplified from Bd21-3 genomic DNA using primers PAN1fwd and PAN1rev and cloned into pENTR/dTOPO (Invitrogen). Then, the clone was digested with AscI (New England Biolabs) and an annealed, double-stranded oligo consisting of Ala_linker-F and Ala_linker-R was ligated in at the C-terminus of the protein. Finally, the resulting construct was re-digested with AscI, and an AscI-flanked Citrine-YFP was ligated in to form the complete construct BdPAN1gene-Alalinker-CitrineYFP pENTR. The Citrine YFP fragment was released by AscI digest from a clone in pJET (Fermentas), which had been originally generated by amplifying the Citrine YFP sequence with primers AscI_FP_noATG-1F and AscI_FP_stop-1R off of plasmid pRSETB-CitrineYFP (Griesbeck et al., 2001). Separately, the BdPAN1 promoter was amplified from Bd21-3 genomic DNA using primers PAN1profwd and PAN1prorev and cloned into pCR8/GW/TOPO. It was subsequently digested out using AscI and ligated into AscI-cut destination vector pIPKb001 (Himmelbach et al., 2007) to generate BdPAN-1pro-pIPKb001. BdPAN1gene-Alalinker-CitrineYFP pENTR was then transferred into this destination vector via LR reaction (Invitrogen) to generate the final construct.

Cortical division site marker *BdTAN1* reporter: To clone *BdPOLARp:BdTAN1-mCitrine* construct, Gibson Assembly was performed according to the Gibson Assembly® Master Mix Kit catalogue (New England Biolabs). priDZ123 and priDZ124, priDZ125 and priDZ126 were used to amplify *BdPOLAR* promoter and *BdTAN1* gene from Bd21-3 genomic DNA, respectively. priDZ127 and priDZ128 were used to amplify mCitrine fragments from pGGD009 (Linker-mCitrine). A total of 0.3 pMol of DNA fragments from *BdPO-LAR* promoter, *BdTAN1* gene, and mCitrine were assembled into backbone pIPK001t. The pIPK001t was digested with OliI and HindIII at 37ºC O/N to remove the Gateway cassette and linearize the backbone. The products of the Gibson reactions were analysed by colony PCR, test digestion, and Sanger sequencing of the whole inserts.

All primer sequences can be found in Table S2.

Generation and Analysis of Transgenic Lines.

Brachypodium calli originated from Bd21-3, *bdmute*, Cas9-negative *bdpolar-1*, and *bdpan1-1* plants were transformed with the AGL1 *Agrobacterium tumefaciens* strain combining the protocols of (Alves et al., 2009; Bragg et al., 2012, 2015). In short, young, transparent embryos were isolated and grown for three weeks on callus induction media (CIM; per L: 4.43g Linsmaier & Skoog basal media (LS; Duchefa #L0230), 30g sucrose, 600µl CuSO$_4$ (1mg/ml, Sigma/Merck #C3036), 500µl 2,4-D (5mg/ml in 1M KOH, Sigma/Merck #D7299), pH 5.8, plus 2.1g of Phytagel (Sigma/Merck #P8169)). After three weeks of incubation at 28ºC in the dark, crisp, yellow callus pieces were subcultured to fresh CIM plates and incubated for two more weeks at 28ºC in the dark. After two weeks, calli were broken down to 2-5mm small pieces and subcultured for one more week at 28ºC in the dark. For transformation, AGL1 Agrobacteria with the desired construct were dissolved in liquid CIM media (same media as above without the phytagel) with freshly added 2,4-D (2.5µg/ml final conc.), Acetosyringone (200µM final conc., Sigma/Merck #D134406), and Synperonic PE/F68 (0.1% final conc., Sigma/Merck #81112). The OD600 of the Agrobacteria solution was adjusted to 0.6. Around 100 calli were incubated for at least 10min in the Agrobacteria solution, dried off on sterile filter paper and incubated for three days at room temperature in the dark. After three days, transformed calli were moved to selection media (CIM + Hygromycin (40µg/ml final conc., Roche #10843555001) + Timentin (200µg/ml final conc., Ticarcillin 2NA & Clavulanate Potassium from Duchefa #T0190)) and incubated for one week at 28ºC in the dark. After one week, calli were moved to fresh selection plates and incubated for two more weeks at 28ºC in the dark. Next, calli were moved to callus regeneration media (CRM; per L: 4.43g of LS, 30g maltose (Sigma/Merck #M5885), 600µl CuSO$_4$ (1mg/ml), pH 5.8, plus 2.1g of Phytagel). After autoclaving, cool down and add Timentin (200µg/ml final conc.), Hygromycin (40µg/ml final conc.), and sterile Kinetin solution (0.2µg/ml final conc., Sigma/Merck #K3253). Calli were incubated at 28ºC and a 16h light:8h dark cycle (70-80 µmol PAR m^{-2} s^{-1}). After 1-6 weeks in the light, shoots will form. Move shoots that are longer than 1cm and ideally have two or more leaves, to rooting cups (Duchefa #S1686) containing rooting media (per L: 4.3g Murashige &Skoog including vitamins (Duchefa #M0222), 30g sucrose, adjust pH to 5.8, add 2.1g Phytagel). After autoclaving cool down and add Timentin (200µg/ml final concentration). Once roots have formed, plantlets can be moved to soil (consisting of 4 parts ED CL73 (Einheitserde) and 1 part Vermiculite) and grown in a greenhouse with 18h light:6h dark cycle (250-350 µmol PAR m^{-2} s^{-1}). Ideally, the transgenic plantlets moved to soil are initially kept at lower temperatures (day temperature = 22ºC, night temperature = 18-20ºC) for 2-4 weeks until they have rooted sufficiently before being moved to the warmer greenhouse (day temperature = 28ºC, night temperature = 22ºC). Gene-edited CRISPR T0 lines were identified by

phenotyping and Sanger sequencing of the edited base pairs; reporter T0 lines were verified by examining the signal from fluorescent molecules.

In-depth analysis was done in subsequent generations that went through the seed stage (T1-T3). For *bdpolar* CRISPR mutants, we generated 1 *bdpolar-1*, 1 *bdpolar-2*, and 3 *bdpolar-3* fertile T1 lines, respectively. For *BdPOLAR* reporters from wild type, we obtained 2 translational *BdPOLARp:BdPOLAR-mVenus* T1 lines, 3 transcriptional *BdPOLARp:3XNLS-eGFP* T1 lines, and 5 C-terminal tagged overexpression *ZmUbip:BdPOLAR-mVenus* independent T1 lines that were fertile and produced seeds. *BdPOLARp:BdPOLAR-mVenus* in *bdmute* was generated by introducing *BdPOLARp:BdPOLAR-mVenus* into *bdmute* calli. For *BdTAN1* reporters in wild-type, *bdpolar-1* and *bdpan1-1,* we obtained 5, 3 and 3 fertile T1 lines, respectively.

Crossing.

To cross *Brachypodium* we followed the illustrated guide from John P Vogel (DOE-JGI) (link) with slight modifications. We inspected the plants grown in soil between 4-5 weeks and selected those in a proper stage for crossing (florets just before anther dehiscence and with fully developed, feathery stigma). For male parents, 20 or more mature anthers per line were collected on a slide and incubated at 28° C for 10-50 mins to induce dehiscence. During the incubation, emasculation was carried out in female parents with fully developed and feathery stigmas. Then pollination was performed by brushing the dehised anther across the stigma with tweezers. A small piece of tape was then applied at the tip of the flower to ensure that the palea and lemma are tightly closed. 10-30 flowers were pollinated per cross. Reporter lines were always used as pollen donors so signals in the F1 generation indicated a successful cross. In the F2, we genotyped the mutant alleles and screened for reporter signals to identify required individuals for analysis. *BdPOLARp:BdPOLAR-mVenus* and *BdPAN1p:BdPAN1-YFP* were crossed as males with *bdpan1-1* and *bdpolar-1* to generate *bdpan1-1;BdPOLARp:BdPOLAR-mVenus* and *bdpolar-1 ;BdPAN1p:BdPAN1-YFP,* respectively. *BdPOLARp:BdPOLAR-mVenus* and *BdPAN1p:BdPAN1-YFP* were crossed as males with *bdpolar-1* and *bdpan1-1* to generate complementation lines *bdpolar-1;BdPOLARp:BdPOLAR-mVenus* and *bdpan1-1;BdPAN1p:BdPAN1-YFP,* respectively.

Microscopy and Phenotyping

Light microscopy for phenotyping of mature stomatal complexes. For DIC imaging, the 3rd leaves of soil-grown plants (17~19 dpg) were collected and fixed in 7:1 ethanol:acetic acid overnight to clear the chlorophyll. The cleared leaves were then rinsed in water and mounted on slides in Hoyer's solution (Liu and Meinke, 1998). For good optical clearing, leaves were usually incubated for 12-24 h on the slide before microscopic analysis. The abaxial side was inspected under a 40X objective using Differential Interference Contrast (DIC) on a Leica DM5000B (Leica Microsystems) and 10-11 fields of view from each individual were saved as pictures for phenotyping SC defects in silico. SCs with transverse or oblique divisions but not correct longitudinal divisions were defined as defective SCs. The numbers of defective SCs and total SCs were counted and recorded simultaneously from each picture. For each defective SC, the frequency of SC divided was counted to distinguish and classify SC division categories (Fig. 4H). To quantify stomata density, 4 abaxial fields (0.290 mm² field of view) per leaf were captured using the 20X objective. The GC length was measured from the top middle point to the bottom middle point of the GC using the "straight" tool in Fiji. The stomata density and GC length were quantified using the leaf areas that were used for stomatal conductance measurements in Fig. 5.

Confocal microscopy. For confocal imaging, the 2nd or 3rd leaf of plate-grown seedlings (5-6 dpg and 8-10 dpg, respectively) were carefully pulled out to reveal the developmental zone (first 2mm at the leaf base), which is covered by the sheaths of older leaves. Samples were stained with propidium iodide (PI, 10 μg/ml, Thermofisher) for approximately 5 min to visualise the cell outlines (i.e. the cell walls), then mounted on a slide with water. Imaging was performed using 63X glycerol immersion objective in Leica TCS SP8 microscope (Leica Microsystems). Image analysis and processing were carried out in Fiji (Schindelin et al., 2012).

Polarity Index.

For Polarity Measurement (POME) (Gong et al. 2020) analysis of BdPAN1-YFP and BdPOLAR-mVenus polarity in WT and mutant backgrounds, confocal images of the developmental zone of 2nd (5~6 dpg) PI-stained leaves were acquired with a 63x glycerol immersion objective and a 2x zoom factor. Individual SMCs at stage three with strong and clear reporter signals were selected for the analysis. 19 to 33 SMCs were analysed for each genotype. For the BdPOLAR reporter lines, only cells with signal at the apical, basal and distal PM were picked. Additionally, recently and incorrectly divided SMCs in both mutant backgrounds were excluded. In some instances where the SMCs were slightly skewed, a small z-stack was obtained and then projected to reveal the complete polarity domain before POME analysis. Fluorescence intensity at each pixel and angle were obtained in ImageJ/FIJI as described by (Gong et al. 2020). Before running POME on a selected cell, the input parameters were specified for each individual cell in the POME FIJI macro. The obtained measurements were then imported, summarised and analysed in RStudio (details available in Gong et al. 2020). The polarity index was calculated as the fraction of fluorescence intensity values above the half maximum (Gong et al. 2021). Briefly, the maximum fluorescence intensity of each cell was determined, and the fraction of values above half of this maximum was calculated. The polarity indices of

all analysed cells of the same condition were grouped and statistically compared to the other conditions with unpaired Mann-Whitney U-tests.

Nuclear migration assay

For nuclear staining experiments, we used the basal 0.5~1 cm developmental zone from 2nd (5-6 dpg) leaves. Firstly, leaf strips were rinsed with 1xPBST 3 times for 10 min each in vials, then 1ng/ml Hoechst 33342 (Thermofisher) solution was added into vials and vacuum was applied 3 times for 10 min each. Then leaf strips in vials were incubated for 1h at room temperature along with gentle shaking. Afterwards, we washed leaf strips with 1xPBST 3 times for 10 min each, then added 0.1% Direct red 23 (w/v) (Sigma-Aldrich) into vials and applied vacuum 3 times for 10 min each, then incubated leaf strips 1h at room temperature along with gentle shaking. Next, we washed leaf strips again with 1xPBST 3 times for 10 min each. Finally, leaf strips were dried with paper and mounted in 50% Glycerol on slides. Direct red 23 and Hoechst 33342 were used to stain the cell wall and nuclei, respectively. Images were captured with the following excitation (Ex) and emission (Em) wavelengths (Ex/Em): Direct red 23 561 nm/600–650 nm and Hoechst 33342 405 nm/425–475 nm. Image analysis and processing were carried out in Fiji. The d distance, GMC length and width were measured in Fiji using the "straight" tool. The d distance was measured starting from the middle point of nuclei in SMC and ending at the middle point of the GMC/SMC interface. The GMC length was measured from the middle point of the apical side to the middle point of the basal side of the GMC. The GMC width was measured from the middle point of the left side to the middle point of the right side of the GMC. To avoid deviations of d distance measurement due to imaging at different Z-axis positions, we also measured the nuclear diameters per genotype, and they did not show a significant difference (Fig. S5B).

Gas exchange measurements.

Leaf-level gas exchange measurements were performed as described in (Nunes et al., 2022). In short, LI-6800 Portable Photosynthesis System (Li-COR Biosciences Inc.) was used to measure the youngest, fully expanded leaf (17-21 days after sowing). The LI-6800 was equipped with a Multiphase Flash Fluorometer (6800-01A) chamber head and the conditions were as follows: flow rate, 500 µmol s^{-1}; fan speed, 10000 rpm; leaf temperature, 28ºC; relative humidity (RH), 40 %; [CO_2], 400 µmol mol^{-1}; photosynthetic active radiation (PAR), 1000 − 100 − 1000 − 0 µmol PAR m^{-2} s^{-1} (20 min per light step). Stomatal conductance (g_{sw}) measurements were automatically logged every minute (Sup Table S3). Relative g_{sw} was computed for each individual measured by normalising g_{sw} to the maximum g_{sw} value observed to assess the kinetics of stomatal response by excluding variation in absolute g_{sw}. 5 individuals each genotype *bdpolar-1*, *bdpan1-1*, *bdpolar-1;bdpan1-1* and 5 individual wild-type were measured. Stomatal opening and closure speed was evaluated by rate constants (k, min^{-1}) determined from exponential equations fitted for each of the three light transitions (1000-100, 100-1000 and 1000-0 PAR), as described in (Nunes et al., 2022).

Statistical Analysis and Plotting.

Statistical analysis was performed in R and GraphPad. For multiple comparisons, one-way ANOVA was applied to determine whether the means of all groups are statistically significantly different. Then a Tukey posthoc test was applied to map out which groups are different from other groups. Significant differences are indicated by different letters. For comparisons between two groups, we used either an unpaired Mann-Whitney U-test or a Welch two-sample t-test as indicated in the figure legends. Significant differences are indicated by asterisks. All plots were done in R using ggplot2 or basic R plotting commands. Plots of stomatal conductance (g_{sw}), relative g_{sw} and exponential regressions were done in GraphPad Prism version 9.1.0.

Zhang et al.

REFERENCES

Alves, S.C., Worland, B., Thole, V., Snape, J.W., Bevan, M.W., and Vain, P. (2009). A protocol for Agrobacterium-mediated transformation of Brachypodium distachyon community standard line Bd21. Nat. Protoc. *4*, 638–649.

Bragg, J.N., Wu, J., Gordon, S.P., Guttman, M.E., Thilmony, R., Lazo, G.R., Gu, Y.Q., and Vogel, J.P. (2012). Generation and characterization of the Western Regional Research Center Brachypodium T-DNA insertional mutant collection. PLoS One *7*, e41916.

Bragg, J.N., Anderton, A., Nieu, R., and Vogel, J.P. (2015). Brachypodium distachyon. Methods Mol. Biol. *1223*, 17–33.

Cartwright, H.N., Humphries, J.A., and Smith, L.G. (2009). PAN1: a receptor-like protein that promotes polarization of an asymmetric cell division in maize. Science *323*, 649–651.

Čermák, T., Curtin, S.J., Gil-Humanes, J., Čegan, R., Kono, T.J.Y., Konečná, E., Belanto, J.J., Starker, C.G., Mathre, J.W., Greenstein, R.L., et al. (2017). A Multipurpose Toolkit to Enable Advanced Genome Engineering in Plants. Plant Cell *29*, 1196–1217.

Cleary, A.L., and Smith, L.G. (1998). The Tangled1 gene is required for spatial control of cytoskeletal arrays associated with cell division during maize leaf development. Plant Cell *10*, 1875–1888.

Debernardi, J.M., Tricoli, D.M., Ercoli, M.F., Hayta, S., Ronald, P., Palatnik, J.F., and Dubcovsky, J. (2020). A GRF–GIF chimeric protein improves the regeneration efficiency of transgenic plants. Nat. Biotechnol. *38*, 1274–1279.

Dong, J., MacAlister, C.A., and Bergmann, D.C. (2009). BASL controls asymmetric cell division in Arabidopsis. Cell *137*, 1320–1330.

Facette, M.R., Park, Y., Sutimantanapi, D., Luo, A., Cartwright, H.N., Yang, B., Bennett, E.J., Sylvester, A.W., and Smith, L.G. (2015). The SCAR/WAVE complex polarizes PAN receptors and promotes division asymmetry in maize. Nat Plants *1*, 14024.

Facette, M.R., Rasmussen, C.G., and Van Norman, J.M. (2019). A plane choice: coordinating timing and orientation of cell division during plant development. Curr. Opin. Plant Biol. *47*, 47–55.

FAO Statistical Pocketbook, F.A.O. (2015). World Food and Agriculture (2015) (Food and Agriculture Organization of the United Nations).

Franks, P.J., and Farquhar, G.D. (2007). The mechanical diversity of stomata and its significance in gas-exchange control. Plant Physiol. *143*, 78–87.

Galatis, B., and Apostolakos, P. (2004). The role of the cytoskeleton in the morphogenesis and function of stomatal complexes. New Phytol. *161*, 613–639.

Giannoutsou, E., Apostolakos, P., and Galatis, B. (2016). Spatio-temporal diversification of the cell wall matrix materials in the developing stomatal complexes of Zea mays. Planta *244*, 1125–1143.

Gong, Y., Alassimone, J., Varnau, R., Sharma, N., Cheung, L.S., and Bergmann, D.C. (2021a). Tuning self-renewal in the Arabidopsis stomatal lineage by hormone and nutrient regulation of asymmetric cell division. Elife *10*, e63335.

Gong, Y., Varnau, R., Wallner, E.-S., Acharya, R., Bergmann, D.C., and Cheung, L.S. (2021b). Quantitative and dynamic cell polarity tracking in plant cells. New Phytol. *230*, 867–877.

Gray, A., Liu, L., and Facette, M. (2020). Flanking Support: How Subsidiary Cells Contribute to Stomatal Form and Function. Front. Plant Sci. *11*, 881.

Griesbeck, O., Baird, G.S., Campbell, R.E., Zacharias, D.A., and Tsien, R.Y. (2001). Reducing the environmental sensitivity of yellow fluorescent protein. Mechanism and applications. J. Biol. Chem. *276*, 29188–29194.

Guo, X., Wang, L., and Dong, J. (2021a). Establishing asymmetry: stomatal division and differentiation in plants. New Phytol. *232*, 60–67.

Guo, X., Park, C.H., Wang, Z.-Y., Nickels, B.E., and Dong, J. (2021b). A spatiotemporal molecular switch governs plant asymmetric cell division. Nat Plants *7*, 667–680.

Haas, A.S., and Raissig, M.T. (2020). Seed Sterilization and Seedling Growth on Plates in the Model Grass Brachypodium distachyon. Bio-Protocol e3700–e3700.

Herrmann, A., Livanos, P., Lipka, E., Gadeyne, A., Hauser, M.-T., Van Damme, D., and Müller, S. (2018). Dual localized kinesin-12 POK 2 plays multiple roles during cell division and interacts with MAP 65-3. EMBO Rep. *19*, e46085.

Hetherington, A.M., and Woodward, F.I. (2003). The role of stomata in sensing and driving environmental change. Nature *424*, 901–908.

Himmelbach, A., Zierold, U., Hensel, G., Riechen, J., Douchkov, D., Schweizer, P., and Kumlehn, J. (2007). A set of modular binary vectors for transformation of cereals. Plant Physiol. *145*, 1192–1200.

Houbaert, A., Zhang, C., Tiwari, M., Wang, K., de Marcos Serrano, A., Savatin, D.V., Urs, M.J., Zhiponova, M.K., Gudesblat, G.E., Vanhoutte, I., et al. (2018). POLAR-guided signalling complex assembly and localization drive asymmetric cell division. Nature *563*, 574–578.

Humphries, J.A., Vejlupkova, Z., Luo, A., Meeley, R.B., Sylvester, A.W., Fowler, J.E., and Smith, L.G. (2011). ROP GTPases act with the receptor-like protein PAN1 to polarize asymmetric cell division in maize. Plant Cell *23*, 2273–2284.

Lampropoulos, A., Sutikovic, Z., Wenzl, C., Maegele, I., Lohmann, J.U., and Forner, J. (2013). GreenGate---a novel, versatile, and efficient cloning system for plant transgenesis. PLoS One *8*, e83043.

Lawson, T., and Vialet-Chabrand, S. (2019). Speedy stomata, photosynthesis and plant water use efficiency. New Phytol. *221*, 93–98.

Lipka, E., Gadeyne, A., Stöckle, D., Zimmermann, S., De Jaeger, G., Ehrhardt, D.W., Kirik, V., Van Damme, D., and Müller, S. (2014). The Phragmoplast-Orienting Kinesin-12 Class Proteins Translate the Positional Information of the Preprophase Band to Establish the Cortical Division Zone in Arabidopsis thaliana. Plant Cell *26*, 2617–2632.

Liu, C.M., and Meinke, D.W. (1998). The titan mutants of Arabidopsis are disrupted in mitosis and cell cycle control during seed development. Plant J. *16*, 21–31.

Livanos, P., and Müller, S. (2019). Division Plane Establishment and Cytokinesis. Annu. Rev. Plant Biol. *70*, 239–267.

Livanos, P., Giannoutsou, E., Apostolakos, P., and Galatis, B. (2015). Auxin as an inducer of asymmetrical division generating the subsidiary cells in stomatal complexes of Zea mays. Plant Signal. Behav. *10*, e984531.

Livanos, P., Galatis, B., and Apostolakos, P. (2016). Deliberate ROS production and auxin synergistically trigger the asymmetrical division

generating the subsidiary cells in Zea mays stomatal complexes. Protoplasma *253*, 1081–1099.

Love, M.I., Huber, W., and Anders, S. (2014). Moderated estimation of fold change and dispersion for RNA-seq data with DESeq2. Genome Biol. *15*, 550.

Lupanga, U., Röhrich, R., Askani, J., Hilmer, S., Kiefer, C., Krebs, M., Kanazawa, T., Ueda, T., and Schumacher, K. (2020). The Arabidopsis V-ATPase is localized to the TGN/EE via a seed plant-specific motif. Elife *9*, e60568.

MacAlister, C.A., Ohashi-Ito, K., and Bergmann, D.C. (2007). Transcription factor control of asymmetric cell divisions that establish the stomatal lineage. Nature *445*, 537–540.

Martinez, P., Luo, A., Sylvester, A., and Rasmussen, C.G. (2017). Proper division plane orientation and mitotic progression together allow normal growth of maize. Proc. Natl. Acad. Sci. U. S. A. *114*, 2759–2764.

McAusland, L., Vialet-Chabrand, S., Davey, P., Baker, N.R., Brendel, O., and Lawson, T. (2016). Effects of kinetics of light-induced stomatal responses on photosynthesis and water-use efficiency. New Phytol. *211*, 1209–1220.

Miao, J., Guo, D., Zhang, J., Huang, Q., Qin, G., Zhang, X., Wan, J., Gu, H., and Qu, L.-J. (2013). Targeted mutagenesis in rice using CRISPR-Cas system. Cell Res. *23*, 1233–1236.

Müller, S., Han, S., and Smith, L.G. (2006). Two Kinesins Are Involved in the Spatial Control of Cytokinesis in Arabidopsis thaliana. Current Biology *16*, 888–894.

Muroyama, A., and Bergmann, D. (2019). Plant Cell Polarity: Creating Diversity from Inside the Box. Annu. Rev. Cell Dev. Biol. *35*, 309–336.

Muroyama, A., Gong, Y., and Bergmann, D.C. (2020). Opposing, Polarity-Driven Nuclear Migrations Underpin Asymmetric Divisions to Pattern Arabidopsis Stomata. Curr. Biol. *30*, 4467–4475.e4.

Nan, Q., Liang, H., Mendoza, J., Liu, L., Fulzele, A., Wright, A., Bennett, E.J., Rasmussen, C.G., and Facette, M.R. (2021). The OPAQUE1/DISCORIDA2 myosin XI is required for phragmoplast guidance during asymmetric cell division in maize. bioRxiv. doi:10.1101/2021.08.29.458084

Nance, J., and Zallen, J.A. (2011). Elaborating polarity: PAR proteins and the cytoskeleton. Development *138*, 799–809.

Nir, I., Amador, G., Gong, Y., Smoot, N.K., Cai, L., Shohat, H., and Bergmann, D.C. (2022). Evolution of polarity protein BASL and the capacity for stomatal lineage asymmetric divisions. Curr. Biol. *32*, 329–337.e5.

Nunes, T.D.G., Zhang, D., and Raissig, M.T. (2020). Form, development and function of grass stomata. Plant J. *101*, 780–799.

Nunes, T.D.G., Slawinska, M.W., Lindner, H., and Raissig, M.T. (2022). Quantitative effects of environmental variation on stomatal anatomy and gas exchange in a grass model. Quantitative Plant Biology *3*, e6.

Pillitteri, L.J., Peterson, K.M., Horst, R.J., and Torii, K.U. (2011). Molecular profiling of stomatal meristemoids reveals new component of asymmetric cell division and commonalities among stem cell populations in Arabidopsis. Plant Cell *23*, 3260–3275.

Raissig, M.T., Abrash, E., Bettadapur, A., Vogel, J.P., and Bergmann, D.C. (2016). Grasses use an alternatively wired bHLH transcription factor network to establish stomatal identity. Proc. Natl. Acad. Sci. U. S. A.

113, 8326–8331.

Raissig, M.T., Matos, J.L., Anleu Gil, M.X., Kornfeld, A., Bettadapur, A., Abrash, E., Allison, H.R., Badgley, G., Vogel, J.P., Berry, J.A., et al. (2017). Mobile MUTE specifies subsidiary cells to build physiologically improved grass stomata. Science *355*, 1215–1218.

Ramalho, J.J., Jones, V.A.S., Mutte, S., and Weijers, D. (2022). Pole position: How plant cells polarize along the axes. Plant Cell *34*, 174–192.

Rowe, M.H., Dong, J., Weimer, A.K., and Bergmann, D.C. (2019). A Plant-Specific Polarity Module Establishes Cell Fate Asymmetry in the Arabidopsis Stomatal Lineage. bioRxiv. doi:10.1101/614636

Schindelin, J., Arganda-Carreras, I., Frise, E., Kaynig, V., Longair, M., Pietzsch, T., Preibisch, S., Rueden, C., Saalfeld, S., Schmid, B., et al. (2012). Fiji: an open-source platform for biological-image analysis. Nat. Methods *9*, 676–682.

Spiegelhalder, R.P., and Raissig, M.T. (2021). Morphology made for movement: formation of diverse stomatal guard cells. Curr. Opin. Plant Biol. *63*, 102090.

Stebbins, G.L., and Shah, S.S. (1960). Developmental Studies of Cell Differentiation in the Epidermis of Monocotyledons. II. Cytological Features of Stomatal Development in the Gramineae. Dev. Biol. *2*, 477–500.

Sutimantanapi, D., Pater, D., and Smith, L.G. (2014). Divergent roles for maize PAN1 and PAN2 receptor-like proteins in cytokinesis and cell morphogenesis. Plant Physiol. *164*, 1905–1917.

Waadt, R., Köster, P., Andrés, Z., Waadt, C., Bradamante, G., Lampou, K., Kudla, J., and Schumacher, K. (2020). Dual-Reporting Transcriptionally Linked Genetically Encoded Fluorescent Indicators Resolve the Spatiotemporal Coordination of Cytosolic Abscisic Acid and Second Messenger Dynamics in Arabidopsis. Plant Cell *32*, 2582–2601.

Wang, H., Guo, S., Qiao, X., Guo, J., Li, Z., Zhou, Y., Bai, S., Gao, Z., Wang, D., Wang, P., et al. (2019). BZU2/ZmMUTE controls symmetrical division of guard mother cell and specifies neighbor cell fate in maize. PLoS Genet. *15*, e1008377.

Wright, A.J., Gallagher, K., and Smith, L.G. (2009). discordia1 and alternative discordia1 function redundantly at the cortical division site to promote preprophase band formation and orient division planes in maize. Plant Cell *21*, 234–247.

Wu, Z., Chen, L., Yu, Q., Zhou, W., Gou, X., Li, J., and Hou, S. (2019). Multiple transcriptional factors control stomata development in rice. New Phytol. *223*, 220–232.

Zhang, X., Facette, M., Humphries, J.A., Shen, Z., Park, Y., Sutimantanapi, D., Sylvester, A.W., Briggs, S.P., and Smith, L.G. (2012). Identification of PAN2 by Quantitative Proteomics as a Leucine-Rich Repeat–Receptor-Like Kinase Acting Upstream of PAN1 to Polarize Cell Division in Maize. Plant Cell *24*, 4577–4589.

Zhang, Y., Wang, P., Shao, W., Zhu, J.-K., and Dong, J. (2015). The BASL polarity protein controls a MAPK signaling feedback loop in asymmetric cell division. Dev. Cell *33*, 136–149.